Carbohydrate Polymers 95 (2013) 449–457

Contents lists available at SciVerse ScienceDirect

Carbohydrate Polymers

journal homepage: www.elsevier.com/locate/carbpol

β-Cyclodextrin conjugated magnetic, fluorescent silica core–shell nanoparticles for biomedical applications

Abu Zayed Md. Badruddoza[a,*], Md. Taifur Rahman[b], Sudipa Ghosh[a], Md. Zakir Hossain[c], Jizhong Shi[c], Kus Hidajat[a], Mohammad Shahab Uddin[d,1]

[a] Department of Chemical and Biomolecular Engineering, National University of Singapore, 4 Engineering Drive 4, Singapore 117576, Singapore
[b] School of Chemistry and Chemical Engineering, The Queen's University of Belfast, Belfast BT9 5AG, Northern Ireland, United Kingdom
[c] Cancer Science Institute of Singapore, National University of Singapore, 28 Medical Drive, #02-07, Centre for Life Sciences, Singapore 117456, Singapore
[d] Department of Biotechnology Engineering, Faculty of Engineering, International Islamic University Malaysia, P.O. Box 10, 50728 Kuala Lumpur, Malaysia

ARTICLE INFO

Article history:
Received 3 December 2012
Received in revised form 7 February 2013
Accepted 25 February 2013
Available online 16 March 2013

Keywords:
Multifunctional magnetic nanoparticles
β-Cyclodextrin
Fluorescent imaging
Cell targeting
Hydrophobic drug inclusion

ABSTRACT

We present synthesis of highly uniform magnetic nanocomposite material possessing an assortment of important functionalities: magnetism, luminescence, cell-targeting, and hydrophobic drug delivery. Magnetic particle Fe_3O_4 is encapsulated within a shell of SiO_2 that ensures biocompatibility of the nanocomposite as well as act as a host for fluorescent dye (FITC), cancer-targeting ligand (folic acid), and a hydrophobic drug storage-delivering vehicle (β-cyclodextrin). Our preliminary results suggest that such core–shell nanocomposite can be a smart *theranostic* candidate for simultaneous fluorescence imaging, magnetic manipulation, cancer cell-targeting and hydrophobic drug delivery.

1. Introduction

In recent years, multifunctional nano-materials have attracted enormous interest within the biomedical research community (Gao, Gu, & Xu, 2009). Rational combination of diverse building blocks such as metallic or semiconductor nanomotifs, organic molecules/polymers, biomolecules give rise to composite nanomaterials which exhibit a wide range of diagnostic and therapeutic capabilities; bioimaging, specific cell targeting, drug storage and controlled drug release (Cho et al., 2010; Yang et al., 2010; Yoon et al., 2006). Magnetic nanoparticles evidently are becoming prominent inorganic building blocks of such multifunctional nanocomposites. Because, colloidal magnetic nanoparticles (MNPs), typically iron oxide (Fe_3O_4), exhibit superparamagnetism which can respond to an external magnetic field. The fact that these superparamagnetic materials do not retain any magnetization after removal of the external magnetic field, and thus avoid aggregation, is a clear advantage for in vivo applications (Idée et al., 2007). MNPs can be magnetically guided inside a biological system, for example, artery or tumor by an external magnetic field (Chertok, David, & Yang, 2011) and tracked by magnetic resonance imaging (MRI) (Y. Chen et al., 2010). Moreover, an inorganic (e.g. silica or gold)/non-polymeric organic (e.g. surfactant)/polymer (e.g. PEG, chitosan) coating on the magnetic particles enhances their stability, biocompatibility, as well as expands applicability by integrating more functionalities via physical and/or chemical methods (Gupta & Gupta, 2005).

A shell of silica around MNPs, known as Fe_3O_4@SiO_2 core–shell, constitutes the basic architecture of most multifunctional nanocomposites (Kim et al., 2008; Liong et al., 2008; Lu et al., 2007; Zhang, Wu, Tong, Tang, & Xu, 2009). Because silica is a good biocompatible material and less prone to degradation in a biological environment (Xu et al., 2010; Yoon et al., 2006). The silica shell can be easily functionalized for bioconjugation through various simple methods and it provides a robust platform in biomedical fields for incorporating diverse functionalities into a single entity (Ow et al., 2005). To date most of the magnetic core–shell nanocomposites exhibit typically two or a maximum of three functionalities by combining the magnetic core with a fluorescent organic dye (Lin & Haynes, 2009; Rosenholm et al., 2009) or quantum dot (Li, Choo, Liu, Ding, & Xue, 2008; Sun et al., 2010), cell targeting ligand (Mohapatra, Mallick, Maiti, Ghosh, & Pramanik, 2007; Rosenholm et al., 2009; Sun et al., 2010) or drugs (Xuan et al., 2011), however little attempt has been made to incorporate four functionalities: magnetism, fluorescence, selective cell-targeting and drug storage-delivery in one single platform. We present a novel core–shell

* Corresponding author. Tel.: +65 6516 2099; fax: +65 6779 1934.
E-mail addresses: cheazmb@nus.edu.sg, babu023@yahoo.com (A.Z.Md. Badruddoza), uddinms@iium.edu.my (M.S. Uddin).
[1] Tel.: +603 61966519; fax: +603 61964442.

0144-8617/$ – see front matter © 2013 Elsevier Ltd. All rights reserved.
http://dx.doi.org/10.1016/j.carbpol.2013.02.046

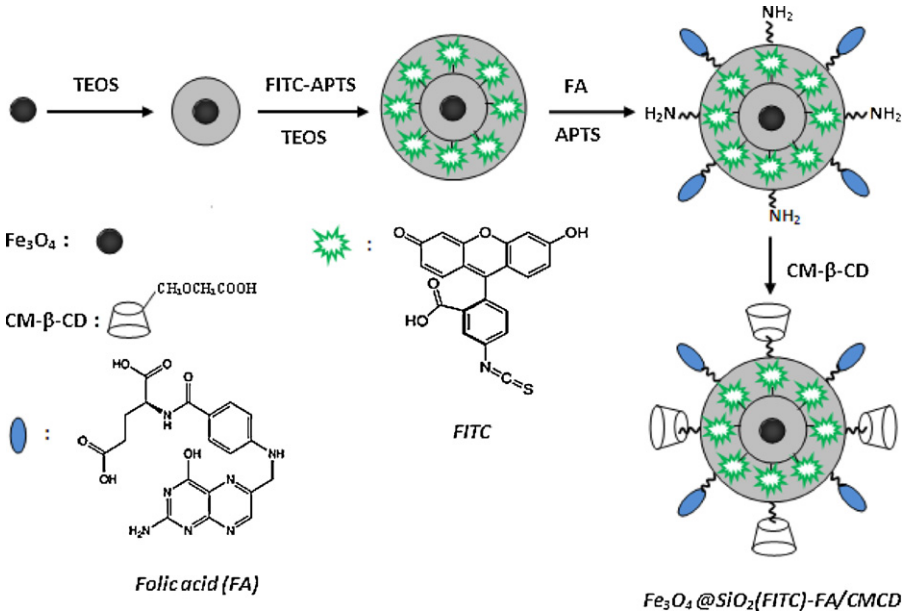

Scheme 1. Synthesis of CM-β-CD conjugated fluorescein-doped magnetic silica nanoparticles [Fe_3O_4@SiO_2(FITC)–FA/CMCD NPs].

nanocomposite which has such *quadruple* of functionalities (Liong et al., 2008).

We rationally design the bottom-up synthesis of a core–shell nanocomposite by stepwise coating of Fe_3O_4 magnetic crystal (~10 nm) with layers of silica shells for colloidal protection, dye-doping and molecular functionalization (Scheme 1). Microemulsion sol–gel chemistry was opted to construct the first layer of silica gel to obtain Fe_3O_4@SiO_2 core–shell structure. We then overlay a fluorescent dye-conjugated (FITC) silica layer to optically track the nanocomposite for any cellular uptake by fluorescence imaging. FITC is chemically encapsulated into the silica shell to enhance photochemical stability (Yoon et al., 2006) and fluorescence intensity due to "caging effects" (Ow et al., 2005). Being both magnetic and fluorescently labeled these materials have the potential for bimodal imaging by optical and magnetic resonance techniques (Corr, Rakovich, & Gun'ko, 2008; Kim et al., 2008; Lin et al., 2006).

For selective delivery of nanoparticulate device, the challenge lies in successfully combining therapeutic and targeting functionalities along with imaging capability into one single nano-system. To this end, the outermost layer of silica is furnished with a cancer cell targeting ligand and an interesting 'molecular cage' for drug storage. We covalently conjugated folic acid to the amino-termini on the outer silica shell. Folic acid or folate (FA) has emerged as an attractive cancer-targeting ligand because cancerous cells overexpress high-affinity FA receptors (FARs) (Yang et al., 2010), thus FA-conjugated nanomaterials show preference toward malignant cells than the healthy ones.

In order to armor our nanocomposite with a drug storage and delivery vehicle we finally conjugated β-cyclodextrin molecules onto the shell. In the magnetic core–shell literature, mesopores in the silica shell are used as the physical reservoir for storing drug molecules (Kim et al., 2008; Liong et al., 2008). However, in most cases these magnetic-mesoporous silica nanocomposites can carry only hydrophilic drugs, because the mesopores of silica can accommodate only water-soluble drug molecules (Baeza, Guisasola, Ruiz-Hernández, & Vallet-Regí, 2012; Y. Chen et al., 2010; Chen, Zhang, Chen, Zhang, & Zhang, 2010; Lee et al., 2010). Unlike physically entrapping drug molecules into the mesopores of silica, we relied on the supramolecular inclusion of drug molecules into the doughnut-shaped β-cyclodextrin (β-CD) cavity. β-CD molecules, a series of cyclic oligosaccharides composed of α(1–4)-linked D-glucopyranose units have a hydrophilic exterior while the internal cavity is sufficiently hydrophobic to host water-insoluble drug molecules (Hayashi et al., 2010; Peng et al., 2010). One of the most remarkable applications of cyclodextrin is its use as drug carriers in controlled release systems. As a drug carrier, β-CD not only facilitates solubilization, stabilization, and transport of hydrophobic drugs but also minimizes unwanted side effects associated with the corresponding drugs (Hedges, 1998; Ramírez et al., 2006; Uekama, Hirayama, & Arima, 2006; Uekama, Hirayama, & Irie, 1998). Several studies have been directed toward constructing MNP-cyclodextrin nanocomposites as magnetically guided drug carrier (Banerjee & Chen, 2007; Cao, He, Deng, & Gao, 2009). However, the agglomeration of these as-synthesized magnetic nanocarriers as evidenced by TEM may limit their applications in biomedical research fields (Banerjee & Chen, 2007, 2008; Cao et al., 2009).

The feasibility of our magnetic nanocomposite as an optically trackable, cancer-cell targeting and delivery vehicle for anticancer drugs is evaluated by investigating their capability in discriminating between cancerous and healthy cells, cellular uptake, fluorescent imaging, formation of hydrophobic drug-inclusion complexes and the in vitro release profile using all-*trans*-retinoic acid (RA) as a model hydrophobic drug. After combining superparamagnetic, luminescent, specific cell-targeting and hydrophobic drug-encapsulation properties, these multi-functional nanoparticles pose great potentials in diverse theranostic applications (Janib, Moses, & MacKay, 2010; Xie, Lee, & Chen, 2010).

2. Experimental

2.1. Materials

All-*trans*-retinoic acid (RA) (98%), 3-aminopropyltriethoxysilane (APTS) (98+%), chloroacetic acid (99%), N-(3-dimethylaminopropyl)-N′-ethylcarbodiimide hydrochloride (EDC), iron (II) chloride tetrahydrate (99%) and iron (III) chloride hexahydrate (98%) were purchased from Alfa Aesar (Singapore). Ammonium hydroxide (25%) was purchased from Merck (USA). 1-hexanol (>98%), oleic acid (99%) and tetraethyl orthosilicate (TEOS) (99%) were purchased from Fluka (Singapore). β-Cyclodextrin

hydrate (99%) was obtained from Sinopharm Chemicals (China). 3-[4,5-Dimethyl-thiazol-2-yl]-2,5-diphenyltetrazolium bromide (MTT), fetal bovine serum (FBS), N-hydroxysuccinimide (NHS), N,N′-dicyclohexylcarbodiimide (DCC) and triton X-100 were purchased from Sigma–Aldrich (Singapore). Folate free Dulbecco's modified Eagle's medium (DMEM) were purchased from Invitrogen Corporation. Fetal bovine serum (FBS) was purchased from Gibco (Life Technologies AG, Switzerland). All other chemicals were used purchased from either Sigma–Aldrich or Fisher Scientific (Singapore) and received without further purification. All the experiments were performed in deionized Milli-Q water.

2.2. Preparation of CM-β-CD

CM-β-CD was prepared following the procedure of literature (Furusaki, Ueno, Sakairi, Nishi, & Tokura, 1996) and the detail synthesis of CM-β-CD was as follows: a mixture of 10 g β-CD and 9.3 g NaOH in 37 mL of water was treated with 27 mL of 16.3% monochloroacetic acid solution at 50 °C for 5 h. Then the reaction mixture was cooled to room temperature, and pH was adjusted (6–7) using hydrochloric acid (2 M). The obtained neutral solution was then poured to superfluous methanol solvent and white precipitates were produced. The resultant product was purified by precipitation with methanol several times until no AgCl precipitation was detected when $AgNO_3$ solution was added to the aqueous solution of the product. The solid precipitation was then filtered and dried under vacuum to give carboxymethylated β-CD (CM-β-CD, 6 g). IR (KBr): ν (cm^{-1}): 3140–3680 (—OH), 2928 (—CH), 1740 (C═O), 960–1200 (C—O—C, C—C/C—O) (Figure S1 in the Supporting Information). The average number of carboxylate groups (3.1) per CM-β-CD was calculated using ^1H NMR (Ravoo, Darcy, Mazzaglia, Nolan, & Gaffney, 2001).

2.3. Preparation of oleic acid coated Fe_3O_4 MNPs

Oleic acid stabilized Fe_3O_4 MNPs were prepared according to the method described by López-López, Durán, Delgado, and González-Caballero (2005). Briefly, 3.04 g $FeCl_3{\cdot}6H_2O$ and 1.26 g $FeCl_2{\cdot}4H_2O$ were dissolved in 50 mL DI water under nitrogen and vigorous stirring with ultrasonification for 10 min. 0.8 mL of oleic acid was then added immediately after 8 mL NH_4OH (25 wt%) had been added to the solution, and the resulting emulsion was stirred vigorously for 1 h at 25 °C. Then the solution was heated up to 95 °C to convert iron hydroxides into magnetite. As soon as that temperature was reached, the suspension was cooled to room temperature. The mixture was then acidified to pH 5–6 with HNO_3 (35%). The resulting magnetic particles were recovered from the reaction mixture by placing the beaker on a permanent Nd–Fe–B magnet. The particles settled within few minutes and were then washed 4–5 times with DI water to remove the unreacted reactants, then washed with ethanol (50 mL) 3 times to remove water and residual oleic acid. Finally the particles were dried in vacuum oven at 50 °C for 3 h.

2.4. Synthesis of Fe_3O_4@SiO_2(FITC) nanoparticles

Typically, 12 mg of dried magnetic Fe_3O_4 powder was dissolved first in 77 mL cyclohexane and then 20 g triton X-100, 16 mL hexanol, and 3.4 mL H_2O were added with intense stirring to generate the microemulsion system (Lu et al., 2007). 0.4 mL of TEOS was added to this mixture. After 6 h of stirring, 1.2 mL aqueous ammonia (25 wt%) was introduced drop wisely to initiate the TEOS hydrolysis. The microemulsion was kept stirring for another 24 h, and then *N*-1-(3-triethoxysilylpropyl)-*N*′-fluoresceyl thiourea (FITC–APTS) ethanolic solution and TEOS (0.3 mL) was added to the microemulsion. FITC–APTS conjugate was prepared by adding 1.25 mg FITC with 0.15 mL APTS in 0.2 mL absolute ethanol and stirring in dark for 24 h in room temperature (Zhang et al., 2009). For FITC–APTS conjugate synthesis, an excess amount of APTS (molar ratio of APTS to FITC = 20) was used to ensure complete conversion of FITC to FITC–APTS conjugates. After stirring in dark for 24 h at room temperature, ethanol was added to destabilize the microemulsion system. The resulting MNPs were collected by magnetic separation and washed 5 times by anhydrous ethanol (20 mL) and then by deionized water to remove surfactant and unreacted reactants and dried by air.

2.5. Synthesis of Fe_3O_4@SiO_2(FITC)–FA/NH_2 nanoparticles

To attach folic acid (FA) to the Fe_3O_4@SiO_2(FITC) MNP surface, FA–APTS conjugate was prepared first. In a flask, 2 mg of FA and 1 μL of APTS were mixed in 20 mL of DMSO. Next, 0.53 mg of NHS and 2.35 mg of DCC (FA:NHS:DCC = 1:1:2.5) were added into the mixture and stirred for 2 h. In a separate flask containing 80 mL of toluene and the Fe_3O_4@SiO_2(FITC) MNPs (50 mg) in DMSO suspension, the FA–APTS conjugate and free APTS (7 μL) (total APTS/FA molar ratio = 8) solution was added, and the mixture was stirred for 20 h at room temperature. The materials were recovered by magnetic separation, washed twice with toluene (20 mL), then ethanol (20 mL) and dried overnight under vacuum.

2.6. Synthesis of Fe_3O_4@SiO_2(FITC)–FA/CMCD nanoparticles

CM-β-CD was grafted onto Fe_3O_4@SiO_2(FITC)–FA/NH_2 NPs in the presence of EDC and NHS. A solution of CM-β-CD (0.65 g, 0.5 mmol) in 20 mL of distilled water was first activated with 0.96 g (0.5 mmol) of EDC and 0.575 g (0.5 mmol) of NHS for 30 min. With this mixture, 100 mg of dried Fe_3O_4@SiO_2(FITC)–FA/NH_2 was added and the pH of the reaction mixture was adjusted to 6–7 by dilute NaOH. The reaction was carried out at room temperature under constant stirring. After 24 h, the product formed was separated by magnetic decantation and dried overnight under vacuum.

2.7. Cell culture and intracellular uptake study

A human cervical carcinoma cell line (HeLa cells) and a human breast adenocarcinoma cell line (MCF-7 cell) were obtained from American Type Culture Collection (ATCC, USA). Passage numbers for MCF-7 and HeLa cells used in this study were 6 and 9, respectively. The HeLa cells were grown in DMEM supplemented with 10% FBS at 37 °C and 5% CO_2. The MCF-7 cells were grown in DMEM supplemented with 10% FBS and 1% insulin (10 mL: 400 U) at 37 °C and 5% CO_2. Cells (5×10^8/L) were plated on 14 mm glass cover slips and allowed to adhere for 24 h. Subsequently, after washing with phosphate buffer solution (PBS), the cells were incubated in PBS buffer containing 100 μg/mL Fe_3O_4@SiO_2(FITC)–FA/CMCD MNPs at 37 °C for 1 h under 5% CO_2, and then washed with PBS sufficiently to remove excess nanoparticles. Nanoparticle uptake by HeLa and MCF-7 cells was studied by confocal microscopy methods. Confocal microscopy images of the cells were acquired with a 488 nm laser on a Leica SP2 confocal laser scanning microscope.

2.8. In vitro cytotoxicity

In vitro cytotoxicity was evaluated by performing methyl thiazolyl tetrazolium (MTT) assays on the HeLa cells. Cells were seeded into a 96-well cell culture plate at 5×10^4 per well in DMEM with 10% FBS at 37 °C and 5% CO_2 for 24 h; then the cells were incubated with Fe_3O_4@SiO_2(FITC)–FA/CMCD NPs with different concentrations (0, 50, 100, 250, 500, and 1000 μg/mL diluted in DMEM) for 48 h at 37 °C under 5% CO_2. Untreated wells were used as control. Thereafter, MTT (10 μl, 5 mg/mL) was added to each well, and the plate was incubated for 4 h at 37 °C. The assays were carried out

according to the manufacturer's instructions. The optical density (OD) value at 570 nm of each well, with background subtraction at 690 nm, was measured by microplate reader (GENios, Tecan, Switzerland).

2.9. Inclusion/adsorption of retinoic acid

The inclusion of RA with Fe_3O_4@SiO_2(FITC)–FA/CMCD NPs was investigated through batch technique (Banerjee & Chen, 2008) by taking precisely 15 mg of Fe_3O_4@SiO_2(FITC)–FA/CMCD NPs in 5 mL of RA solutions of different concentration (0.01–1.5 mM) at pH 9.75 and 25 °C. The stock solution of RA (4.0 mM) was prepared by dissolving 60.1 mg of RA in a mixture containing 5 mL ethanol and 5 mL 0.1 N NaOH solution and then making up the volume with water to 50 mL. For further dilution, phosphate buffer of pH 9.75 was used. The pH of final RA solution was adjusted by 0.1 N NaOH or HCl. The solution was stirred with a thermostatic water-bath shaker (200 rpm) for 12 h (which was the time required for equilibration to be reached) and then the magnetic nanoparticles were removed magnetically from the solution. The concentrations of RA solution were determined using a UV-visible spectrophotometer model UV-1601. The calibration curve of absorbance against different concentrations of RA was made at 341 nm.

2.10. Release study

The drug release experiment was performed in an Erlenmeyer flask at 37 °C in PBS buffer (0.1 M, pH 7.4). 120 mg of Fe_3O_4@SiO_2(FITC)–FA/CMCD NPs containing a known amount of RA were suspended in 250 mL of release medium, stirred at 150 rpm in a thermostatic water-bath heater maintained at 37 °C. 5 mL of samples were periodically removed and assayed. The volume of each sample withdrawn was replaced by the same volume of fresh medium. The amount of released RA was determined at 341 nm using a UV–vis spectrophotometer. The drug release study was performed twice for each of the samples. To prevent decomposition of RA during the release experiment, the samples were kept in dark.

2.11. Physical and chemical analyses of core–shell particles

FTIR measurements were performed in a transmission mode using a Shimadzu infrared spectrometer (Model 8400) with KBr as background over the range of 4000–400 cm^{-1}. Analysis of the chemical composition of as-synthesized nanoparticles was carried out via X-ray photoelectron spectroscopy (XPS) on an AXIS HSi spectrometer (Kratos Analytical Ltd.) using a monochromatized Al Kα X-ray source (1486.6 eV photons) at a constant dwell time of 100 ms and a pass energy of 40 eV. The sample was mounted on the standard sample studs by means of double sided adhesive tape. The core-level signals were obtained at a photoelectron take-off angle 90° (with respect to the sample surface). The anode voltage was 15 kV, and the anode current was 10 mA. The pressure in the analysis chamber was maintained at 6.7×10^{-6} Pa or lower during each measurement. All binding energies (BEs) were referenced to the C1*s* neutral carbon peak at 284.6 eV. Thermogravimetric analysis (TGA) was performed on a TGA 2050 thermogravimetric analyzer (TA Instruments). For TGA measurements, the weight loss of dried sample was monitored under N_2 at temperatures from room temperature to 800 °C at a rate of 10 °C/min. Transmission electron microscopy (TEM) images were recorded on a JEOL 2010 transmission electron microscope at an accelerating voltage of 200 kV. The TEM specimens were prepared by placing a drop of the nanoparticle suspension on a carbon-coated copper grid (200 mesh and cover with formvar/carbon). The copper film was then dried at room temperature for 24 h before the measurement. The zeta potentials were measured on a Malvern ZEN 3600 Zeta-sizer Nano-ZS. The hydrodynamic diameters and corresponding size distribution of particles were measured by dynamic light scattering (DLS) using the same Zeta-sizer instrument.

3. Results and discussion

3.1. Synthesis and characterization of multifunctional magnetic nanoparticles

The synthetic route for multifunctional core–shell magnetic nanoparticles [Fe_3O_4@SiO_2(FITC)–FA/CMCD NPs] is outlined in Scheme 1. Fluorescently doped core–shell structured Fe_3O_4@SiO_2(FITC) NPs was obtained by a one-pot two-step method. In the first step, oleic-acid-stabilized Fe_3O_4 MNPs were coated with a layer of silica to make the basis of the core–shell structure. Fe_3O_4 MNPs were dispersed in a water-in-oil (cyclohexane–hexanol) microemulsion prior to the sol–gel formation of the silica layer onto the magnetite surface. In the second step, this emulsion was further treated with a mixture of FITC–APTS conjugate and free APTS overlay thin FITC-doped silica on the primary shell. The purpose of the primary silica shell is to protect the core Fe_3O_4 MNP. As the dye molecules are incorporated into the second silica layer, any possibility of FITC degradation or fluorescence quenching by Fe_3O_4 is minimized. Secondly, encasing FITC within a thin layer of condensed APTS-layer would provide photostability and additional chemical protection in the cellular environment. The outermost layer of Fe_3O_4@SiO_2(FITC) was then decorated with a cancer targeting ligand, folate by silanization with folic acid–APTS conjugate. A fair excess of APTS (molar ratio of APTS to FA = 10) was used to ensures sufficient free amino groups dangling out from the outer surface for further functionalization. CM-β-CD, the molecular host from hydrophobic drugs was attached onto the outermost surface via amide bond formation between the carboxylic groups of CM-β-CD with free amino groups.

High resolution TEM images of as-prepared multifunctional Fe_3O_4@SiO_2(FITC)–FA/CMCD NPs show that highly monodispersed particles with mean diameter 70 nm (silica shell thickness = 30 nm) are formed (Fig. 1). Moreover, a thin ring on the outer surface can

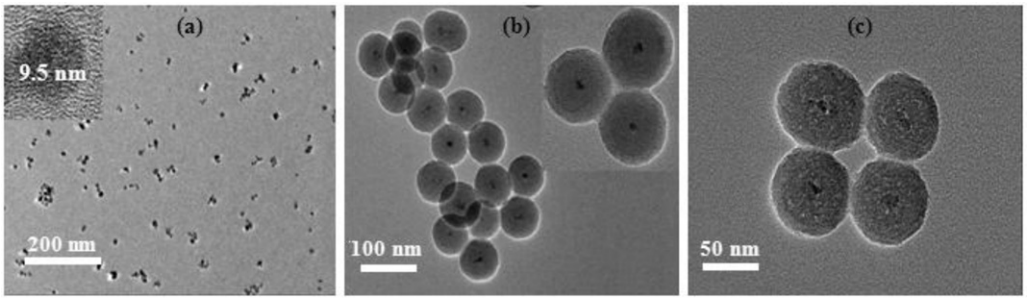

Fig. 1. TEM mages of (a) OA-MNPs, (b) Fe_3O_4@SiO_2(FITC) NPs and (c) Fe_3O_4@SiO_2(FITC)–FA/CMCD NPs.

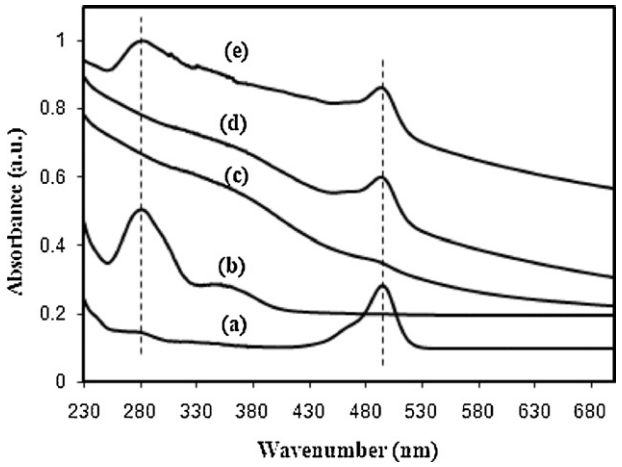

Fig. 2. UV–vis spectra of (a) pure FITC, (b) pure folic acid, (c) Fe_3O_4@SiO_2 NPs, (d) Fe_3O_4@SiO_2(FITC) NPs, and (e) Fe_3O_4@SiO_2(FITC)–FA/NH_2 NPs in water.

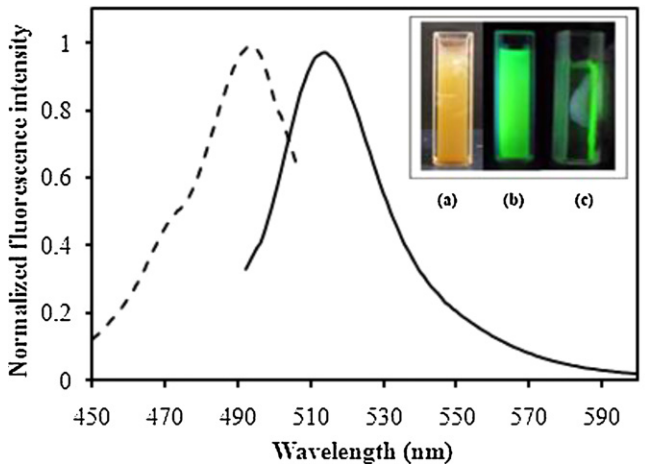

Fig. 3. Excitation (dashed line, recorded at 515 nm emission) and emission (solid line, recorded at 480 nm excitation) spectra of Fe_3O_4@SiO_2(FITC)–FA/CMCD NPs dispersed in water. Insets: visual photographs of (a) Fe_3O_4@SiO_2(FITC) NPs dispersion in water under room light; (b) the green emission of these MNPs in water and (c) in response to a NdFeB magnet under the 365 nm excitation portable UV lamp.

be observed which may be due to the surface organic group (Lu et al., 2007). For each core–shell particle a singular oleic acid coated Fe_3O_4 NP, rather than a cluster, is encased within a thick layer of silica shell. Oleic acid modified Fe_3O_4 MNPs have an average diameter of 9.5 nm. The synthesized highly monodispersed core–shell silica NPs are achieved by microemulsion-based sol–gel growth of silica in limited domain of water in the water-in-oil microemulsion. It can be assumed that the aqueous microdroplets in this microemulsion system are monodisperse in size and each water droplet contains a single MNP around which a well-defined shell of silica is grown through hydrolysis of TEOS and subsequent condensation of silica onto the surface of magnetic cores.

Physical and chemical features of the core–shell multifunctional particles are investigated by several analytical methods. XRD patterns of silica-coated magnetic core–shell particles, i.e., Fe_3O_4@SiO_2(FITC) NPs (Figure S2 in the Supporting Information) shows that peaks corresponding to uncoated Fe_3O_4 are significantly masked, and mergence of a broad peak ranging from 20° to 30° indicates the presence of an amorphous silica shell around Fe_3O_4. However, silica coating does not result in the phase change of Fe_3O_4 nanoparticles. FTIR trace of Fe_3O_4@SiO_2(FITC) NPs (Figure S3 in the Supporting Information) exhibits typical signatures for silica (a strong broad brand at 1090 cm^{-1} corresponding to the Si—O—Si asymmetric stretching vibration and a weak band at 956 cm^{-1} associated to Si—OH vibration) (Yang et al., 2010). The bands at 1630 cm^{-1} and 1560 cm^{-1} are the bending of N—H, characteristic of the presence of NH_2 group. The peak at 2938 cm^{-1} is due to the C—H stretching vibrations of alkyl groups. The SQUID spectrum of Fe_3O_4@SiO_2(FITC)–FA/CMCD NPs (Figure S4 in the Supporting Information) measured at 300 K exhibits no hysteresis loop, which means that these multifunctional nanocomposites retain the superparamagnetic property.

The successful attachment of fluorescent probe molecule (FITC) and cell-targeting ligand (FA) into/onto the silica shell was investigated by UV–vis spectroscopic analyses (Fig. 2). UV–vis absorption spectra of all the samples were measured in aqueous medium. Fe_3O_4@SiO_2 nanocomposites do not show any prominent absorption peaks. Characteristic absorption bands for FITC and FA, at 488 and 280 nm, respectively, are clearly visible in the case of Fe_3O_4@SiO_2(FITC)–FA/NH_2 NPs and are not blue/red shifted due to the integration inside/on a silica matrix (when compared with UV absorptions for free FITC and FA).

The incorporation of FITC dye in Fe_3O_4@SiO_2(FITC)–FA/CMCD NPs enabled the nanoprobes with excellent fluorescent property in water (Fig. 3). The emission spectrum of the dye-doped multifunctional NPs shows a broad band ranging from 490 to 580 nm with a maxima at 515 nm. Fe_3O_4@SiO_2(FITC)–FA/CMCD nanoprobes and pure FITC dye in water has similar excitation and emission spectra (not shown here), so the fluorescent characteristics of FITC dye did not alter after incorporation into a silica-shell. The spectral properties (excitation and emission spectra) of Fe_3O_4@SiO_2(FITC)–FA/CMCD NPs were comparable with FITC dye-doped magnetic silica nanoparticles in the literature (Kim et al., 2008; Yoon et al., 2006). Inset picture in Fig. 3 shows dispersions of these nanoparticles under room light and under the 365 nm UV excitation. Clearly, these core–shell MNPs are highly dispersible in water and emit strong green fluorescence under 365 nm UV excitation. Facile magnetic separation is evident from its magnetic responsivity toward a permanent NdFeB magnet. Moreover, after being harvested by an external magnet, absence of any fluorescence in the aqueous part confirms that FITC is robustly embedded into the silica shell by chemical bonding and does not leach out. In this work FITC was used as a model fluorescence probe, however, other more bio-compatible fluorescent markers, that require longer excitation wavelengths, can be integrated into the core–shell NPs in a similar fashion.

The stepwise conjugation of functional groups on the silica surface was monitored by measuring the surface charges and surface chemistry at different stages of synthesis (Scheme 1). As shown in Fig. 4A, a negative zeta potential (ξ) value of −27 mV (at pH 7.4) of dye-doped silica particles [Fe_3O_4@SiO_2(FITC) NPs], can be attributed to the presence of ionizable silanol groups of surface silica and acid functionalities (COOH and phenolic-OH) of FITC molecules (Santra et al., 2004). After modification with APTS/FA conjugate, the ξ value of Fe_3O_4@SiO_2(FITC)–FA/NH_2 NPs reverts to positive value ($\xi \sim +4.0$ mV at pH 7.4) due to the presence of excess amount of amino groups which exist mainly as NH_3^+ below. FA is expected to furnish silica surface with negative charge, however excess amount of NH_2 groups presumable nullify it, making the overall surface charge slightly positive. Further modification of the surface by conjugating cyclodextrin groups is manifested in the reversal of surface charge back to a negative value −20 mV attributable to the high ionizability of CM-β-CD ($pK_a < 4$) groups. As a result, Fe_3O_4@SiO_2(FITC)–FA/CMCD NPs were observed to be well dispersed in aqueous medium without any visible aggregation (insets of Fig. 3). Good aqueous dispersibility and colloidal stability of the nanoparticles are essential for their biological applications. DLS analyses suggest long-term colloidal stability over a

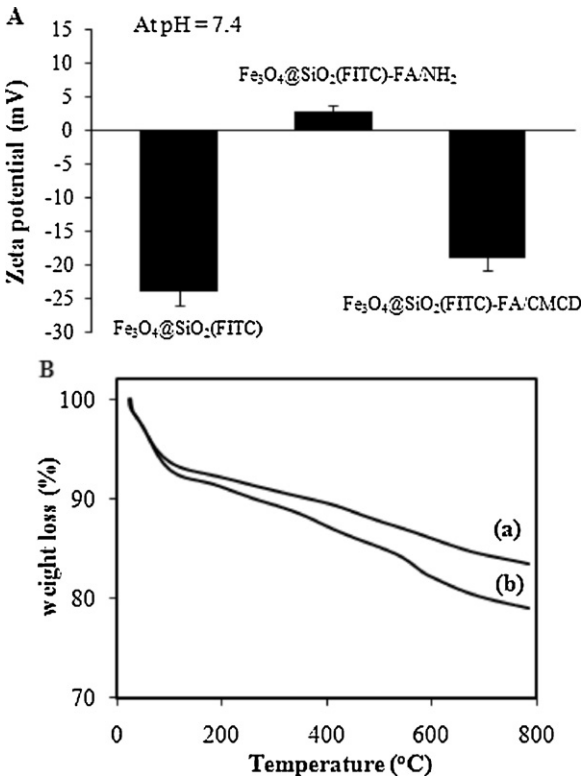

Fig. 4. (A) Zeta potentials of as-synthesized nanoparticles at pH 7.4; (B) TGA curves of (a) Fe_3O_4@SiO_2(FITC)–FA/NH_2 and (b) Fe_3O_4@SiO_2(FITC)–FA/CMCD NPs.

few day time and narrow size distribution (hydrodynamic diameter ~ca. 125 nm and polydispersity index ~ 0.25) (Figure S5 in the Supporting Information).

Successful and step-wise attachment of organic groups onto silica surface is also validated by examining the chemical compositions at each step by XPS. For example, progressive rise in the relative carbon content % on the silica surfaces down this series: Fe_3O_4@SiO_2(FITC), Fe_3O_4@SiO_2(FITC)–FA/NH_2 and Fe_3O_4@SiO_2(FITC)–FA/CMCD NPs, clearly shows that organic functionalities on the surface is gradually enriched by iterative chemical conjugation (Table 1).

High density grafting of cyclodextrin molecules onto the outermost silica surface is desirable as these are the host for hydrophobic drug molecules. TGA curves (25–800 °C) in Fig. 4B shows the weight loss due to organics decomposition in both Fe_3O_4@SiO_2(FITC)–FA/NH_2 and Fe_3O_4@SiO_2(FITC)–FA/CMCD NPs. Though the weight loss trend for both samples is similar, these TGA curves do not approach constant even the temperature increases up to 800 °C. No plausible explanation could be made for such thermal behavior, however, similar observation were recorded earlier (Ku et al., 2010). A comparison of two TGA curves revealed an increased weight loss for Fe_3O_4@SiO_2(FITC)–FA/CMCD NPs, presumably due to the presence of substantial amount of CM-β-CD. The amount of CM-β-CD grafted on the surface was calculated to be 0.034 mmol/g.

3.2. Specific targeting and cellular uptake

After successful synthesis and full physical and chemical characterizations, biomedical relevance of Fe_3O_4@SiO_2(FITC)–FA/CMCD NPs was investigated. We carried out fluorescence imaging of the cellular uptake of these multifunctional NPs for their ability to discriminate between healthy and cancerous cells. After 1 h incubation of HeLa and MCF-7 cells with these NPs at 37 °C, cells were observed using confocal laser scanning microscope (CLSM) (Fig. 5). Corresponding bright field images of the cells were also recorded. A clear preference for the cancerous cells (HeLa) by these MNPs over MCF-7 cells is demonstrated in Fig. 5. Cytoplasm of all HeLa cells (Fig. 5A) is highly fluorescent due to the presence of FITC-tagged MNPs, while most of MCF-7 cells are less or non-invaded by the NPs (by comparing dark and bright field images) under similar conditions. These results corroborate the overexpression of folate receptor on HeLa cells, which may facilitate the recognition of Fe_3O_4@SiO_2(FITC)–FA/CMCD NPs and increase the uptake through internalization, presumably by folate receptor mediated endocytosis (Mohapatra et al., 2007; Yang et al., 2010). This suggests that these multifunctional NPs could be used for targeting and imaging cancerous cells simultaneously.

3.3. Drug inclusion and release studies

Since Fe_3O_4@SiO_2(FITC)–FA/CMCD NPs are capable of preferentially target and invade cancerous cells, use of these particles as an anti-cancer drug carrier would be ideal for tumor-specific drug delivery. In this direction, we investigated drug loading capacity of these multifunctional NPs which are already decorated with well-known molecular drug carrier: β-cyclodextrin. We chose RA as a model hydrophobic anti-cancer drug. In order to get an idea about supramolecular interactions between RA and free CM-β-CD molecules in solution, host–guest type complex formation was investigated by UV–vis spectroscopy. Fig. 6(a) shows the UV–vis spectra of RA (7.3×10^{-6} mol L^{-1}) in 10 vol% methanol solutions (pH 7.4) containing various concentrations of CM-β-CD. Previous studies showed that methanol even up to 20 vol% does not influence the inclusion of cyclodextrin with other guest molecules (Guo, Ren, Fang, & Liu, 1995). The UV absorption peak is shifted to shorter wavelengths with an increase in the CM-β-CD concentrations, accompanied by the increase in absorbance. This indicates the formation of the RA/CM-β-CD inclusion complexes. Similar inclusion behaviors of cyclodextrin with various drugs by UV–vis spectroscopy have been reported in literature (Crupi et al., 2007; Liu, Chen, Chen, & Lin, 2005).

The inclusion constant (K) of RA/CM-β-CD complex is estimated by using the double-reciprocal method as in Eq. (1) (Benesi & Hildebrand, 1949).

$$\frac{1}{\Delta A} = \frac{1}{\alpha} + \frac{1}{\alpha K [CD]_0} \quad (1)$$

where ΔA denotes the difference of absorption of guest molecule in the presence and absence of CDs. α is a constant, and $[CD]_0$ denotes the concentration of CDs. K can be calculated from a plot of $1/\Delta A$ vs. $1/[CD]$. Inset of Fig. 6(a) shows the double reciprocal plots of $1/\Delta A$

Table 1
Surface composition of Fe_3O_4@SiO_2(FITC), Fe_3O_4@SiO_2(FITC)–FA/NH_2 and Fe_3O_4@SiO_2(FITC)–FA/CMCD NPs obtained from XPS spectra.

Samples	Surface elemental composition percentage (%)			
	C 1s	O 1s	Si 2p	N 1s
Fe_3O_4@SiO_2(FITC)	15.62	46.90	36.46	1.02
Fe_3O_4@SiO_2(FITC)–FA/NH_2	16.80	45.76	34.95	2.48
Fe_3O_4@SiO_2(FITC)–FA/CMCD	23.23	45.17	29.57	2.03

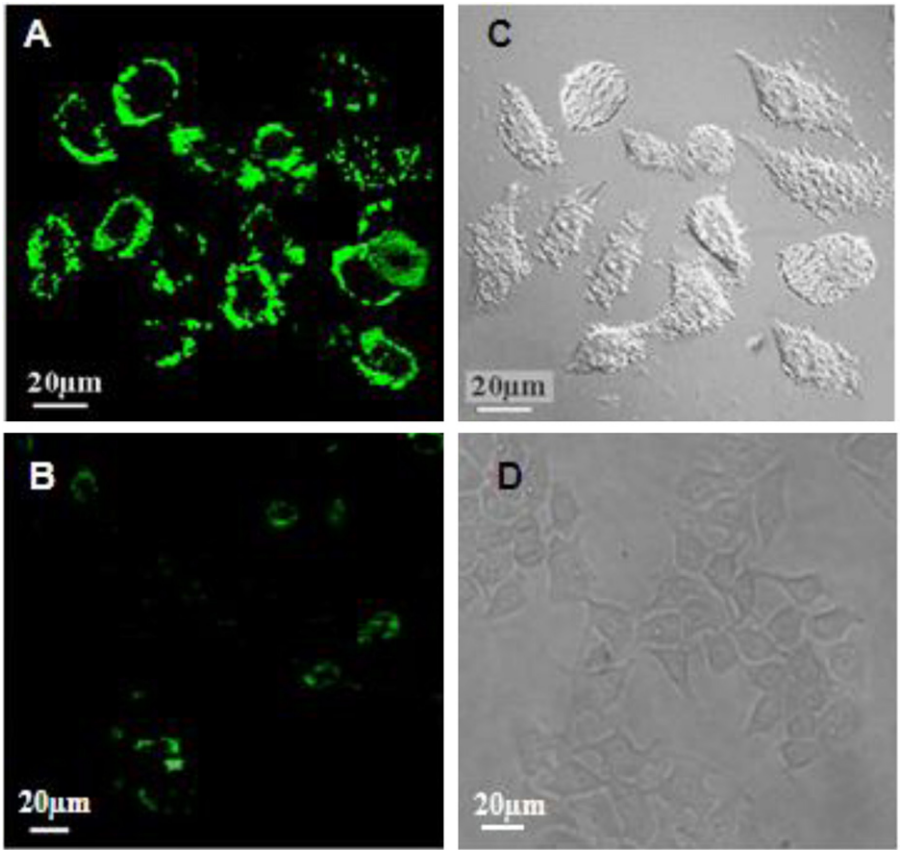

Fig. 5. CLSM images of cells incubated with Fe_3O_4@SiO_2(FITC)–FA/CMCD NPs at 37 °C after 1 h incubation: (A) HeLa cells (FA-positive) and (B) MCF-7 cells (FA-negative). Bright field images of HeLa cells (C) and MCF-7 cells (D) were also supplied.

versus 1/[*CD*] for RA with CM-β-CD at pH 7.4. The plot exhibits good linearity (the linear regression coefficient $R^2 = 0.998$). This verifies the formation of inclusion complexes with a stoichiometry of 1:1 between RA and CM-β-CD. The relative inclusion constant of CM-β-CD with RA is estimated to be 779 M^{-1}. The lipophilic character of RA provides the main driving force for their inclusion into the apolar CDs cavities. Literature values for CD-drug inclusion constant varies from 100 to 10,000 M^{-1} (Challa, Ahuja, Ali, & Khar, 2005). For therapeutic applications, a moderate value for K is desirable that ensures thermodynamic feasibility for drug inclusion in the drug loading stage, while at the same time does not impede drug release when needed (Ascenso et al., 2011).

Encouraged by the extent of RA/CM-β-CD complex formation in molecular level, we determined the capabilities of CM-β-CD-decorated nanocomposites [Fe_3O_4@SiO_2(FITC)–FA/CMCD NPs] to RA drug loading. Fig. 6(b) shows that Fe_3O_4@SiO_2(FITC)–FA/CMCD NPs exhibits considerable adsorption capability for RA compared to nanocomposites without any CM-β-CD functional groups [Fe_3O_4@SiO_2(FITC)–FA/NH_2 NPs] revealing a clear manifestation of cyclodextrin's role as a potent molecular drug carrier in the nanocomposite.

In order to gain more insight into the phenomenon of RA complexation by Fe_3O_4@SiO_2(FITC)–FA/CMCD NPs adsorption equilibrium data are fitted by Langmuir model which can be expressed as (Langmuir, 1918):

$$\frac{C_e}{q_e} = \frac{C_e}{q_m} + \frac{1}{q_m K_L} \quad (2)$$

where q_e is the amount of adsorbed RA at equilibrium (mg/g), C_e the equilibrium RA concentration in solution (mg/L), q_m the maximum adsorption capacity of adsorbent (mg/g), and K_L is the "affinity parameter" or Langmuir constant (L/mg). The values of q_m and K_L are determined from the slope and intercept of the linear plots of C_e/q_e versus C_e (Fig. 6b). The Langmuir isotherm ($R^2 = 0.99$) shows a better fit to experimental data in compared to the Freundlich isotherm ($R^2 = 0.94$) (The Freundlich data are not shown here). From the slope and intercept, the values of q_m and K_L could be determined as 8.30 mg g^{-1} and 0.17 L mg^{-1}.

We then focused on the drug release profile from RA complexed-Fe_3O_4@SiO_2(FITC)–FA/CMCD NPs in PBS (0.1 M, pH 7.4) at 37 °C. Fig. 7 shows the release profiles of RA-loaded Fe_3O_4@SiO_2(FITC)–FA/CMCD NPs (containing 2.5 μmole RA) as a function of time. The typical release profile was characterized by an initial rapid release phase in the first 60 min when almost 23% of the total drug was released. These results suggest that a portion of the total drug–CD complexes in the nanocomposite are quite labile, whereas the rest apparently more stable. Apart from van der Walls interaction between hydrophobic part of RA and CD cavity, at certain conformational arrangements hydrogen bonding between the polar functional groups' of RA and CD and the release of high energy water molecules from the cavity during the complex formation may contribute to further stabilization for some RA–CD complexes, contributing to slow down the release process (Liu & Guo, 2002). Thus the reversible and predictive nature of complex formation with hydrophobic molecules makes CD to serve as a dual agent of drug *loading and unloading* in our nanocomposite. Apart from relying on passive drug release (vide supra), the magnetic core can be exploited for magneto-responsive release of the drug from the MNP surface (Baeza et al., 2012; Timko, Dvir, & Kohane, 2010) which we envisage as a potential research direction toward a remotely controllable, sustained-release of drugs from CD-decorated nanocomposites.

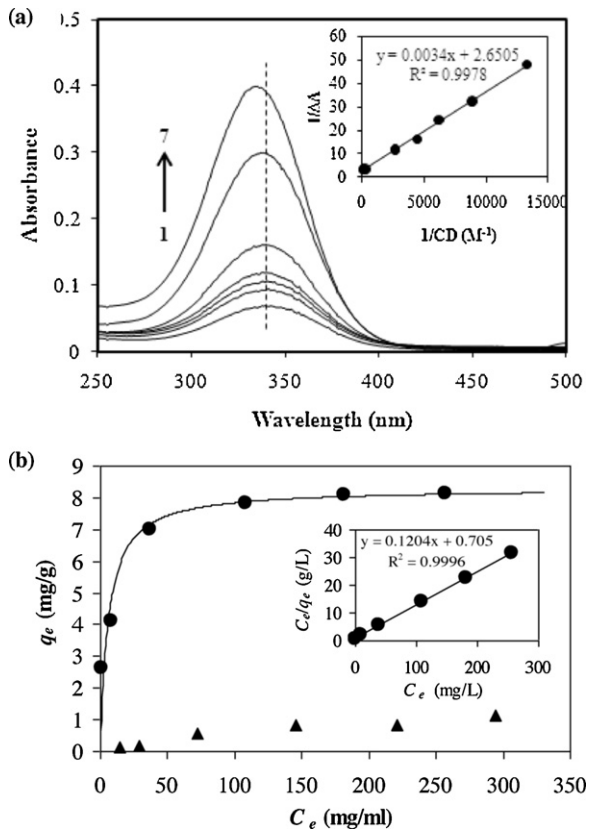

Fig. 6. (a) Absorption spectra of all-*trans*-retinoic acid (RA) (7.3×10^{-6} mol L^{-1}) in pH 7.4 buffer containing various concentrations of CM-β-CD. Concentrations of CM-β-CD: (1) 0, (2) 7.5×10^{-5}, (3) 1.1×10^{-4}, (4) 1.6×10^{-4}, (5) 2.3×10^{-4}, (6) 5.6×10^{-4} and (7) 3.8×10^{-3} mol L^{-1}. Inset: double reciprocal plot for RA complexes with CM-β-CD. (b) Equilibrium isotherms for the adsorption of RA by (●) Fe_3O_4@SiO_2(FITC)–FA/CMCD NPs and (▲) Fe_3O_4@SiO_2(FITC)–FA/NH_2 NPs. Inset: illustration of the linear dependence of C_e/q_e on C_e for the adsorption of RA by Fe_3O_4@SiO_2(FITC)–FA/CMCD NPs.

In the present work the release data were fitted to the Ritger–Peppas equation given as follows (Philip & Ritger, 1987):

$$\frac{M_t}{M_\infty} = kt^n \tag{3}$$

where M_t/M_∞ is the amount of drug released, t is the time of release, k is a kinetic constant, and n is a diffusion exponent which describes the drug release mechanism. For spherical metrics, when $n \leq 0.43$, diffusion is the major driving force, normally termed "Fickian diffusion". When $n > 0.85$ drug release is mainly controlled by degradation, termed case II transport. When the value of n is between 0.43 and 0.85, the drug release mechanism is anomalous. The value of the exponent n is determined from the slope of the linear plot of $\ln(M_t/M_\infty)$ versus $\ln t$. Our experimental data showed a fairly good fit to the Ritger–Peppas equation for RA release as the correlation coefficient (R^2) is 0.972. The value of n is determined as 0.26, indicating a Fickian diffusion controlled mechanism.

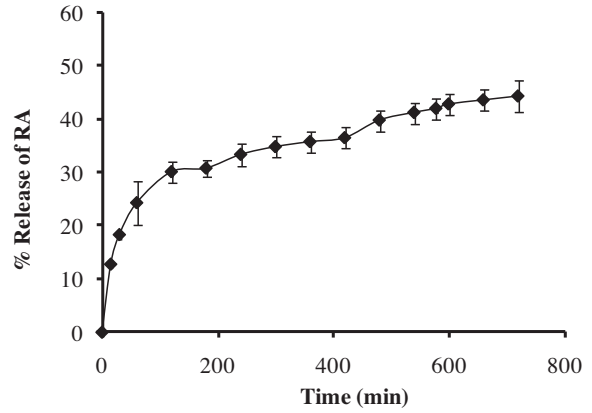

Fig. 7. Release profile of retinoic acid from Fe_3O_4@SiO_2(FITC)–FA/CMCD NPs.

3.4. Cytotoxicity assay

The in vitro cytotoxicity of Fe_3O_4@SiO_2(FITC)–FA/CMCD NPs was evaluated using an MTT assay using the HeLa and MCF-7 cell line. As shown in Figure S6(a), these cell lines still maintained greater than 80% cell viability after 48 h of treatment with Fe_3O_4@SiO_2(FITC)–FA/CMCD NPs at concentrations as high as 1000 μg/mL. These nanocomposites have a low level of cytotoxicity on both HeLa and MCF-7 cells confirming their biocompatibility over a broad concentration range. The cytotoxic effect of the drug loaded nanocomposites was also tested on the HeLa cell line. Figure S6(b) shows the cytotoxicity of free RA and RA loaded Fe_3O_4@SiO_2(FITC)-FA/CMCD NPs at different RA concentrations toward HeLa cells. When treated with an equivalent concentration of RA, both free RA and RA-loaded Fe_3O_4@SiO_2(FITC)–FA/CMCD NPs showed a moderately growth inhibition for HeLa cells in a dose dependent manner. Furthermore, HeLa cancer cells show slightly lower viability by treatment with RA-loaded nanocomposites than free RA at higher RA concentration. This suggests that these RA-loaded NPs can increase the cellular uptake and efficiently deliver the drug to the cells due to the high cellular internalization of FA-conjugated nanocomposites via receptor binding endocytosis (Liong et al., 2008).

4. Conclusion

We synthesized highly uniform and monodispersed multifunctional magnetic nanocomposite that is capable of performing a quadruple of activities: magnetic manipulation, bioimaging, cell-targeting, drug storing-and-releasing. The synthesis involves several stages of covalent attachments of functional molecules and ligands orchestrated in rational way to ensure the chemical robustness. All functional groups were capable of performing independently being within one single nanosystem. Our magnetically maneuverable nanocomposite shows to be highly dispersible in aqueous medium and benign toward healthy cells. Folate ligand leads to preferential internalization into the target cancerous cells. Fluorescence tag acts as a beacon to know the whereabouts of the particles within a cell and the cyclodextrin moiety can carry and release drug pay-load in a biologically relevant environment. Magnetic core material has two other features which could further expand the potency of our nanocomposite: magnetic resonance would facilitate in vivo imaging (MRI) and magneto-responsive drug release should enable a remotely controllable and sustained drug-delivery system.

Acknowledgement

AZMB acknowledges the Research Scholarship of National University of Singapore. This work was financially supported by the National University of Singapore Research Fund (R279-000-003-001).

Appendix A. Supplementary data

Supplementary data associated with this article can be found, in the online version, at http://dx.doi.org/10.1016/j.carbpol.2013.02.046.

References

Ascenso, A., Guedes, R., Bernardino, R., Diogo, H., Carvalho, F. A., Santos, N. C., et al. (2011). Complexation and full characterization of the tretinoin and dimethyl-beta-cyclodextrin complex. *AAPS PharmSciTech*, *12*, 553–563.

Baeza, A., Guisasola, E., Ruiz-Hernández, E., & Vallet-Regí, M. (2012). Magnetically triggered multidrug release by hybrid mesoporous silica nanoparticles. *Chemistry of Materials*, *24*(3), 517–524.

Banerjee, S. S., & Chen, D. H. (2007). Magnetic nanoparticles grafted with cyclodextrin for hydrophobic drug delivery. *Chemistry of Materials*, *19*, 6345–6349.

Banerjee, S. S., & Chen, D. H. (2008). Cyclodextrin conjugated magnetic colloidal nanoparticles as a nanocarrier for targeted anticancer drug delivery. *Nanotechnology*, *19*, 265601–265607.

Benesi, H. A., & Hildebrand, J. H. (1949). *Journal of American Chemical Society*, *71*, 2703.

Cao, H., He, J., Deng, L., & Gao, X. (2009). Fabrication of cyclodextrin-functionalized superparamagnetic Fe_3O_4/amino-silane core–shell nanoparticles via layer-by-layer method. *Applied Surface Science*, *255*, 7974–7980.

Challa, R., Ahuja, A., Ali, J., & Khar, R. (2005). Cyclodextrins in drug delivery: An updated review. *AAPS Pharmscitech*, *6*(2), 329–357.

Chen, F. H., Zhang, L. M., Chen, Q. T., Zhang, Y., & Zhang, Z. J. (2010). Synthesis of a novel magnetic drug delivery system composed of doxorubicin-conjugated Fe_3O_4 nanoparticle cores and a PEG-functionalized porous silica shell. *Chemical Communications*, *46*(45), 8633–8635.

Chen, Y., Chen, H., Zeng, D., Tian, Y., Chen, F., Feng, J., et al. (2010). Core/shell structured hollow mesoporous nanocapsules: A potential platform for simultaneous cell imaging and anticancer drug delivery. *ACS Nano*, *4*(10), 6001–6013.

Chertok, B., David, A. E., & Yang, V. C. (2011). Brain tumor targeting of magnetic nanoparticles for potential drug delivery: Effect of administration route and magnetic field topography. *Journal of Controlled Release*, *155*(3), 393–399.

Cho, H. S., Dong, Z., Pauletti, G. M., Zhang, J., Xu, H., Gu, H., et al. (2010). Fluorescent, superparamagnetic nanospheres for drug storage, targeting, and imaging: A multifunctional nanocarrier system for cancer diagnosis and treatment. *ACS Nano*, *4*(9), 5398–5404.

Corr, S. A., Rakovich, Y. P., & Gun'ko, Y. K. (2008). Multifunctional magnetic-fluorescent nanocomposites for biomedical applications. *Nanoscale Research Letters*, *3*(3), 87–104.

Crupi, V., Ficarra, R., Guardo, M., Majolino, D., Stancanelli, R., Venuti, V., et al. (2007). UV–vis and FTIR–ATR spectroscopic techniques to study the inclusion complexes of genistein with beta-cyclodextrins. *Journal of Pharmaceutical and Biomedical Analysis*, *44*(1), 110–117.

Furusaki, E., Ueno, Y., Sakairi, N., Nishi, N., & Tokura, S. (1996). Facile preparation and inclusion ability of a chitosan derivative bearing carboxymethyl-β-cyclodextrin. *Carbohydrate Polymers*, *29*(1), 29–34.

Gao, J., Gu, H., & Xu, B. (2009). Multifunctional magnetic nanoparticles: Design, synthesis, and biomedical applications. *Accounts of Chemical Research*, *42*(8), 1097–1107.

Guo, Q. X., Ren, T., Fang, Y. P., & Liu, Y. C. (1995). Binding of vitamin A by β-cyclodextrin and heptakis(2,6-O-dimethyl)-β-cyclodextrin. *Journal of Inclusion Phenomena and Molecular Recognition in Chemistry*, *22*, 251–256.

Gupta, A. K., & Gupta, M. (2005). Synthesis and surface engineering of iron oxide nanoparticles for biomedical applications. *Biomaterials*, *26*, 3995–4021.

Hayashi, K., Ono, K., Suzuki, H., Sawada, M., Moriya, M., Sakamoto, W., et al. (2010). High-frequency, magnetic-field-responsive drug release from magnetic nanoparticle/organic hybrid based on hyperthermic effect. *ACS Applied Materials & Interfaces*, *2*(7), 1903–1911.

Hedges, A. R. (1998). Industrial applications of cyclodextrins. *Chemical Reviews*, *98*(5), 2035–2044.

Idée, J. M., Port, M., Raynal, I., Schaefer, M., Bonnemain, B., Prigent, P., et al. (2007). *The superparamagnetic iron oxides nanoparticles for magnetic resonance imaging applications*. Weinheim, Germany: Wiley–VCH.

Janib, S. M., Moses, A. S., & MacKay, J. A. (2010). Imaging and drug delivery using theranostic nanoparticles. *Advanced Drug Delivery Reviews*, *62*(11), 1052–1063.

Kim, J., Kim, H., Lee, N., Kim, T., Kim, H., Yu, T., et al. (2008). Multifunctional uniform nanoparticles composed of a magnetite nanocrystal core and a mesoporous silica shell for magnetic resonance and fluorescence imaging and for drug delivery. *Angewandte Chemie International Edition*, *47*(44), 8438–8441.

Ku, S., Yan, F., Wang, Y., Sun, Y., Yang, N., & Ye, L. (2010). The blood–brain barrier penetration and distribution of PEGylated fluorescein-doped magnetic silica nanoparticles in rat brain. *Biochemical and Biophysical Research Communications*, *39*, 871–876.

Langmuir, I. (1918). The adsorption of gases on plane surfaces of glass, mica and platinum. *Journal of American Chemical Society*, *40*, 1361–1403.

Lee, J. E., Lee, N., Kim, H., Kim, J., Choi, S. H., Kim, J. H., et al. (2010). Uniform mesoporous dye-doped silica nanoparticles decorated with multiple magnetite nanocrystals for simultaneous enhanced magnetic resonance imaging, fluorescence imaging, and drug delivery. *Journal of the American Chemical Society*, *132*(2), 552–557.

Li, L., Choo, E. S. G., Liu, Z., Ding, J., & Xue, J. (2008). Double-layer silica core–shell nanospheres with superparamagnetic and fluorescent functionalities. *Chemical Physics Letters*, *461*(1-3), 114–117.

Lin, Y. S., & Haynes, C. L. (2009). Synthesis and characterization of biocompatible and size-tunable multifunctional porous silica nanoparticles. *Chemistry of Materials*, *21*(17), 3979–3986.

Lin, Y. S., Wu, S. H., Hung, Y., Chou, Y. H., Chang, C., Lin, M. L., et al. (2006). Multifunctional composite nanoparticles: Magnetic, luminescent, and mesoporous. *Chemistry of Materials*, *18*(22), 5170–5172.

Liong, M., Lu, J., Kovochich, M., Xia, T., Ruehm, S. G., Nel, A. E., et al. (2008). Multifunctional inorganic nanoparticles for imaging, targeting, and drug delivery. *ACS Nano*, *2*(5), 889–896.

Liu, L., & Guo, Q. X. (2002). The driving forces in the inclusion complexation of cyclodextrins. *Journal of Inclusion Phenomena and Macrocyclic Chemistry*, *42*, 1–14.

Liu, Y., Chen, G. S., Chen, Y., & Lin, J. (2005). Inclusion complexes of azadirachtin with native and methylated cyclodextrins: Solubilization and binding ability. *Bioorganic & Medicinal Chemistry*, *13*(12), 4037–4042.

Lu, C. W., Hung, Y., Hsiao, J. K., Yao, M., Chung, T. H., Lin, Y. S., et al. (2007). Bifunctional magnetic silica nanoparticles for highly efficient human stem cell labeling. *Nano Letters*, *7*(1), 149–154.

López-López, M. T., Durán, J. D. G., Delgado, A. V., & González-Caballero, F. (2005). Stability and magnetic characterization of oleate-covered magnetite ferrofluids in different nonpolar carriers. *Journal of Colloid and Interface Science*, *291*(1), 144–151.

Mohapatra, S., Mallick, S. K., Maiti, T. K., Ghosh, S. K., & Pramanik, P. (2007). Synthesis of highly stable folic acid conjugated magnetite nanoparticles for targeting cancer cells. *Nanotechnology*, *18*(38), 385102–385110.

Ow, H., Larson, D. R., Srivastava, M., Baird, B. A., Webb, W. W., Wiesner, U., et al. (2005). Bright and stable core–shell fluorescent silica nanoparticles. *Nano Letters*, *5*(1), 113–117.

Peng, K., Cui, C., Tomatsu, I., Porta, F., Meijer, A. H., Spaink, H. P., et al. (2010). Cyclodextrin/dextran based drug carriers for a controlled release of hydrophobic drugs in zebrafish embryos. *Soft Matter*, *6*(16), 3778.

Philip, L., & Ritger, N. A. P. (1987). A simple equation for description of solute release. II. Fickian and anomalous release from swellable devices. *Journal of Controlled Release*, *5*, 37–42.

Ramírez, H. L., Valdivia, A., Cao, R., Torres-Labandeira, J. J., Fragoso, A., Villalonga, R., et al. (2006). Cyclodextrin-grafted polysaccharides as supramolecular carrier systems for naproxen. *Bioorganic & Medicinal Chemistry Letters*, *16*(6), 1499–1501.

Ravoo, B. J., Darcy, R., Mazzaglia, A., Nolan, D., & Gaffney, K. (2001). Supramolecular tapes formed by a catanionic cyclodextrin in water. *Chemical Communications*, *9*, 827–828.

Rosenholm, J. M., Meinander, A., Peuhu, E., Niemi, R., Eriksson, J. E., Sahlgren, C., et al. (2009). Targeting of porous hybrid silica nanoparticles to cancer cells. *ACS Nano*, *3*(1), 197–206.

Santra, S., Yang, H., Dutta, D., Stanley, J. T., Holloway, P. H., Tan, W., et al. (2004). TAT conjugated, FITC doped silica nanoparticles for bioimaging applications. *Chemical Communications*, *24*, 2810–2811.

Sun, L., Zang, Y., Sun, M., Wang, H., Zhu, X., Xu, S., et al. (2010). Synthesis of magnetic and fluorescent multifunctional hollow silica nanocomposites for live cell imaging. *Journal of Colloid and Interface Science*, *350*(1), 90–98.

Timko, B. P., Dvir, T., & Kohane, D. S. (2010). Remotely triggerable drug delivery systems. *Advanced Materials*, *22*(44), 4925–4943.

Uekama, K., Hirayama, F., & Arima, H. (2006). Recent aspect of cyclodextrin-based drug delivery system. *Journal of Inclusion Phenomena and Macrocyclic Chemistry*, *56*, 3–8.

Uekama, K., Hirayama, F., & Irie, T. (1998). Cyclodextrin drug carrier systems. *Chemical Reviews*, *98*(5), 2045–2076.

Xie, J., Lee, S., & Chen, X. (2010). Nanoparticle-based theranostic agents. *Advanced Drug Delivery Reviews*, *62*(11), 1064–1079.

Xu, Z., Li, C., Kang, X., Yang, D., Yang, P., Hou, Z., et al. (2010). Synthesis of a multifunctional nanocomposite with magnetic, mesoporous, and near-IR absorption properties. *The Journal of Physical Chemistry C*, *114*(39), 16343–16350.

Xuan, S., Wang, F., Lai, J. M. Y., Sham, K. W. Y., Wang, Y. X. J., Lee, S. F., et al. (2011). Synthesis of biocompatible, mesoporous Fe_3O_4 nano/microspheres with large surface area for magnetic resonance imaging and therapeutic applications. *ACS Applied Materials & Interfaces*, *3*(2), 237–244.

Yang, H., Zhuang, Y., Hu, H., Du, X., Zhang, C., Shi, X., et al. (2010). Silica-coated manganese oxide nanoparticles as a platform for targeted magnetic resonance and fluorescence imaging of cancer cells. *Advanced Functional Materials*, *20*, 1733–1742.

Yoon, T., Yu, K., Kim, E., Kim, J., Kim, B., Yun, S., et al. (2006). Specific targeting, cell sorting, and bioimaging with smart magnetic silica core–shell nanomaterials. *Small*, *2*(2), 209–215.

Zhang, R., Wu, C., Tong, L., Tang, B., & Xu, Q.-H. (2009). Multifunctional core–shell nanoparticles as highly efficient imaging and photosensitizing agents. *Langmuir*, *25*(17), 10153–10158.